High-pressure crystallography of rhombohedral $PrAlO_3$ perovskite

2009 J. Phys.: Condens. Matter 21 235403

(http://iopscience.iop.org/0953-8984/21/23/235403)

J. Phys.: Condens. Matter **21** (2009) 235403 (9pp) doi:10.1088/0953-8984/21/23/235403

High-pressure crystallography of rhombohedral $PrAlO_3$ perovskite

Jing Zhao[1], Nancy L Ross[1], Ross J Angel[1], Michael A Carpenter[2], Christopher J Howard[2,3], Dorota A Pawlak[4] and Tadeusz Lukasiewicz[4]

[1] Virginia Tech Crystallography Laboratory, Department of Geosciences, Virginia Polytechnic Institute and State University, Blacksburg, VA 24060, USA
[2] Department of Earth Sciences, University of Cambridge, Downing Street, Cambridge CB2 3EQ, UK
[3] School of Engineering, The University of Newcastle, Callaghan, NSW 2308, Australia
[4] Institute of Electronic Materials Technology, ulica Wolczynska 133, 01-919 Warsaw, Poland

E-mail: jzhao@vt.edu

Received 6 January 2009, in final form 23 April 2009
Published 18 May 2009
Online at stacks.iop.org/JPhysCM/21/235403

Abstract

The evolution of the crystal structure of rhombohedral $PrAlO_3$ perovskite with pressure has been investigated by single-crystal x-ray diffraction and Raman scattering experiments. The structural evolution as indicated by lattice strains, octahedral tilts, and the distortions of the octahedral AlO_6 and polyhedral PrO_{12} groups with increasing pressure, is controlled by the relative compressibilities of the AlO_6 octahedra and the PrO_{12} site. Because the AlO_6 octahedra are more compressible than the PrO_{12} sites, up to 7.4 GPa the structure evolves towards the high-symmetry cubic phase like any other rhombohedral perovskite. The variation of volume of the rhombohedral phase with pressure can be represented by a third-order Birch–Murnaghan equation of state with bulk modulus $K_0 = 193.0(1.2)$ GPa and $K' = 6.6(4)$. Above 7.4 GPa the evolution towards a cubic phase is interrupted by a phase transition. Observations are consistent with the assignment of $Imma$ symmetry to the high-pressure phase. Comparison with the low-temperature $R\bar{3}c$ to $Imma$ transition confirms that electronic interactions stabilize the $Imma$ phase.

1. Introduction

Structural phase transitions in perovskites that involve both octahedral tilting and cation displacements are the basis of many ferroelectric materials. The high-pressure phase transition behavior of ferroelectric perovskites should, in principal, provide important insights into the interactions that control the commercially important properties of these materials. For example, high pressure can be used to suppress the dynamics of chemically and micro-structurally complex relaxor ferroelectrics and allow the tilt transitions to be characterized in more detail than is possible at ambient pressures (Mihailova *et al* 2008). Yet, in structurally simpler perovskites such as $PbTiO_3$, in which the symmetry rules for the possible phase transitions are constrained by theory (Howard and Stokes 2005), the phase transition sequence itself at high pressures remains a matter of experimental controversy (Ahart *et al* 2008, Janolin *et al* 2008) and the mechanisms uncertain (Frantti *et al* 2007). This is surprising given that the structures of perovskites are simple enough for conceptual understanding at the crystal-chemical level, but have just enough degrees of freedom (Hammonds *et al* 1998) to enable them to display complex transition behavior.

Of the perovskites, those with $R\bar{3}c$ symmetry provide an ideal model system because the structure can be described in terms of just three free parameters; two cell parameters and one variable fractional coordinate of the oxygen atom. The positions of the octahedral cation, B, and the extra-framework (nominally 12-coordinate) A cation are fixed on symmetry positions. Nonetheless the symmetry constraints do allow the octahedra to tilt around one axis, to compress, and to distort, as in other perovskite space groups (Megaw and Darlington 1975). In the hexagonal setting of the unit-cell, the A cation is at (0, 0, 1/4), the B cation is at (0, 0, 0), and the oxygen is at

$(x, 0, 1/4)$. The tilt angle ω of the octahedra around the three-fold axis is given by (Megaw and Darlington 1975):

$$\omega = \arctan[2\sqrt{3}(x - 0.5)]. \quad (1)$$

The tilt angle becomes zero in the cubic aristotype phase with $Pm\bar{3}m$ symmetry which can be achieved at high temperatures (Howard *et al* 2000). The tilt angle can also be expressed in terms of the ratio of the polyhedral volumes as (Thomas 1996):

$$V_A/V_B = 6\cos^2\omega - 1. \quad (2)$$

Differentiation of this equation shows that changes in the tilt of the octahedra with pressure are therefore controlled by the difference in volume compressibility $(\beta_B - \beta_A)$ between the BO_6 octahedra and AO_{12} polyhedra (Zhao *et al* 2004b):

$$\frac{d\omega}{dP} = -\frac{6\cos^2\omega - 1}{6\sin 2\omega}(\beta_B - \beta_A). \quad (3)$$

On the basis of bond-valence theory, it can be shown (Zhao *et al* 2004a) that in a perovskite with cations with formal charge +3 the BO_6 octahedra are more compressible than the extra-framework AO_{12} polyhedra. That is, $(\beta_B - \beta_A) > 0$ and the tilt angle ω of $R\bar{3}c$ perovskites should decrease with increasing pressure, meaning that the structure should evolve towards cubic symmetry. This has been observed experimentally for $LaAlO_3$ (Bouvier and Kreisel 2002), and in *ab initio* computer simulations of $RAlO_3$ (R = La, Nd, Sm, and Gd) and $LaGaO_3$ at higher pressures (Tohei *et al* 2005). However, a powder XRD study suggested that pressure induces a first-order phase transition from $R\bar{3}c$ to $Imma$ symmetry in $PrAlO_3$ perovskite (Kennedy *et al* 2002). The question therefore arises as to whether $PrAlO_3$ is an exception to the general rules governing compression of perovskites (Zhao *et al* 2004a), or whether factors other than octahedral tilting contribute to the high-pressure behavior. In this contribution, we report a high-pressure structural study of $PrAlO_3$ by high-resolution single-crystal x-ray diffraction that resolves this issue.

2. Experimental method

A relatively large single crystal from a batch grown by the Czochralski method (Pawlak *et al* 2005) was polished to a plate about 23 μm thick and cut into smaller pieces approximately 60 μm × 100 μm for high-pressure experiments. No twin domains were observed by optical microscopy. The absence of twins was confirmed by the observation of sharp and unsplit x-ray diffraction maxima. The unit-cell parameters and refined structure at ambient pressure are consistent with those previously reported (Howard *et al* 2000, Kennedy *et al* 2002).

The selected crystal (60 μm × 100 μm × 23 μm) was loaded on to the 600 μm diameter culet of one anvil of an ETH diamond anvil cell (Miletich *et al* 2000). A 200 μm thick T301 steel gasket was pre-indented to a thickness of 90 μm and a hole ($\varnothing$ = 300 μm) was drilled in the center of the indented region. A 4:1 methanol:ethanol mixture served as the pressure-transmitting medium. A ruby sphere (~20 μm) and quartz crystal were loaded together with the crystal as the internal pressure calibrants (Angel *et al* 1997, Mao *et al* 1986). All unit-cell parameters up to ~7 GPa (table 1a) were determined by a least-squares fit to the corrected setting angles of 15–20 reflections measured by the eight-position centering technique (Angel *et al* 1997) on a Huber four-circle diffractometer.

Table 1a. Unit-cell parameters of $PrAlO_3$ perovskite at high pressure.

P (GPa)	a (Å)	c (Å)	V (Å^3)
0.0001	5.333 13(16)	12.972 9(4)	319.544(19)
0.700(3)	5.326 87(12)	12.957 5(3)	318.417(20)
1.407(6)	5.320 51(15)	12.942 9(4)	317.298(19)
2.094(4)	5.314 56(10)	12.927 76(27)	316.219(12)
3.060(5)	5.306 47(13)	12.907 7(4)	314.769(16)
3.904(6)	5.299 57(12)	12.891 6(3)	313.560(15)
4.859(5)	5.291 69(10)	12.873 06(28)	312.178(13)
5.896(7)	5.283 49(15)	12.854 7(4)	310.768(18)
6.567(6)	5.278 29(21)	12.842 9(6)	309.871(26)
6.965(7)	5.275 53(23)	12.835 75(23)	309.374(28)

Intensity data for all accessible reflections were collected at room pressure (in air and in the DAC) and at different pressures for the sample using ω scans in the fixed-φ mode (Finger and King 1978) from 2° to 40° in θ on an Xcalibur-I diffractometer (Oxford Diffraction) with Mo Kα radiation and a point detector. The offsets of the crystal from the rotation axis of the goniometer were determined by measuring twenty to forty strong low-angle reflections and calculating the crystal offsets from the reflection positions with the WinIntegrStp program, v3.5 (Angel 2003). These offsets were minimized by adjusting the DAC on the goniometer before data collection. Peak fitting and integration of data collection scans were carried out with the WinIntegrStp 3.5 software. Other data corrections including absorption by the sample itself, the diamond anvils and the beryllium plates of the DAC as well as shadowing by the gasket were made by ABSORB 6.0 (Angel 2004). After the crystallographically equivalent reflections were averaged, the remaining independent reflections with $(F^2 > 2\sigma(F^2))$ were used to refine structures with RFINE99, a development version of RFINE4 (Finger and Prince 1975). Unit-cell parameters measured on the Huber diffractometer were used in the structure refinements. Refinement information and parameters for the sample in the DAC at ambient pressure are listed in tables 1a and 2a–2c. A second set of high-pressure experiments was subsequently performed with a second loading of the same crystal, in order to investigate the previously reported phase transition above 7 GPa.

For Raman measurements another piece of the $PrAlO_3$ crystal was loaded along with a ruby ball as the pressure marker into a BR-series DAC (High-Pressure Diamond Optics, Inc) with a 4:1 methanol:ethanol mixture as the pressure medium. The sample was not oriented and unpolarized Raman spectra were then collected in backscattering geometry at room temperature and several pressures with a Jobin-Yvon Horiba LabRam HR800 system, equipped with an electronically cooled charge coupled device (CCD) detection system (1024 × 256) and a grating with 2400 grooves mm^{-1}. The laser beam, emitted from a Laser-physics Reliant 100S-514 nm argon

Table 1b. Bulk moduli of unit-cell volume, axes, and AlO_6 and PrO_{12} polyhedra.

BM EoS fit	K_0 (GPa)	K'	P_{max} (GPa)	χ^2
$V_0 = 313.559(9)$ Å^3	193.0(1.2)	6.6(4)	0.016	0.5
$a_0 = 5.333\,14(12)$ Å	195.0(2.0)	5.5(6)	0.024	0.4
$c_0 = 12.973\,19(29)$ Å	189.8(1.9)	8.7(6)	0.033	1.0
$V_{PrO12} = 44.08(5)$ Å^3	220(15)	4(fixed)	0.8	0.51
$V_{AlO6} = 9.106(9)$ Å^3	182(9)	4(fixed)	0.7	1.08

laser with an output power of 50 mW, was focused onto the sample by an Olympus 10× objective. The laser power at the sample was estimated to be about 3 mW. The width of the monochromator entrance slit was 150 μm.

3. Results and discussion

This section consists of three parts. We first present the elasticity of $PrAlO_3$, the bulk modulus, and the axial bulk moduli, and then we examine the variation of the spontaneous strains with pressure. In section 3.2 we present the structural evolution of $PrAlO_3$, paying special attention to the relative compressibilities of the AlO_6 and PrO_{12} polyhedra, the tilt angle of octahedral AlO_6 and the polyhedral distortions with increasing pressure. Finally the evidence for a high-pressure phase transition is presented.

3.1. Equation of state of $PrAlO_3$ and lattice strains

The unit-cell volume of $PrAlO_3$ perovskite decreases smoothly as a function of pressure without evidence of any phase transition before 7 GPa as shown in figure 1(a), consistent with the high-pressure powder x-ray diffraction data (Kennedy *et al* 2002). A least-squares fit of the P–V data with a third-order Birch–Murnaghan equation of state (EoS) yielded a room pressure bulk modulus of $K_0 = 193.0 \pm 1.2$ GPa and $K' = (\mathrm{d}K/\mathrm{d}P)_{P=0} = 6.6 \pm 0.4$ (table 1b and figure 1(b)). The value of K' is typical of many oxide perovskites (Angel *et al* 2007, Ross *et al* 2004a, 2004b).

We obtained the compressional moduli of the unit-cell axes ($a = b, c$) of $PrAlO_3$ perovskite by fitting a third-order Birch–Murnaghan equation of state to the cubes of a- and c-axial lengths (Angel 2000). At room pressure $PrAlO_3$ is almost elastically isotropic, with $K_{a0} = 195.0(2.0)$ GPa being very slightly stiffer than $K_{c0} = 189.8(1.9)$ GPa. As a consequence the ratio $c/a\sqrt{6}$, which expresses the deviation from cubic lattice symmetry, remains essentially constant at low pressures (figure 2). But at higher pressures, the fact (table 1b and figure 1(c)) that $K'_{c0} = 8.7(6)$ is higher than $K'_{a0} = 5.5(5)$, means that the c-axis becomes stiffer than the a-axis and the ratio $c/a\sqrt{6}$ increases, but at a much slower rate than that observed in the $R\bar{3}c$ perovskite $LaAlO_3$ (figure 2) in which the c-axis is significantly stiffer than the a-axis (Zhao *et al* 2004b).

A complete analysis of the possible phase transitions in $PrAlO_3$ has been made within the framework of Landau theory (Carpenter *et al* 2005) which shows that the spontaneous strain provides the principal coupling between the order

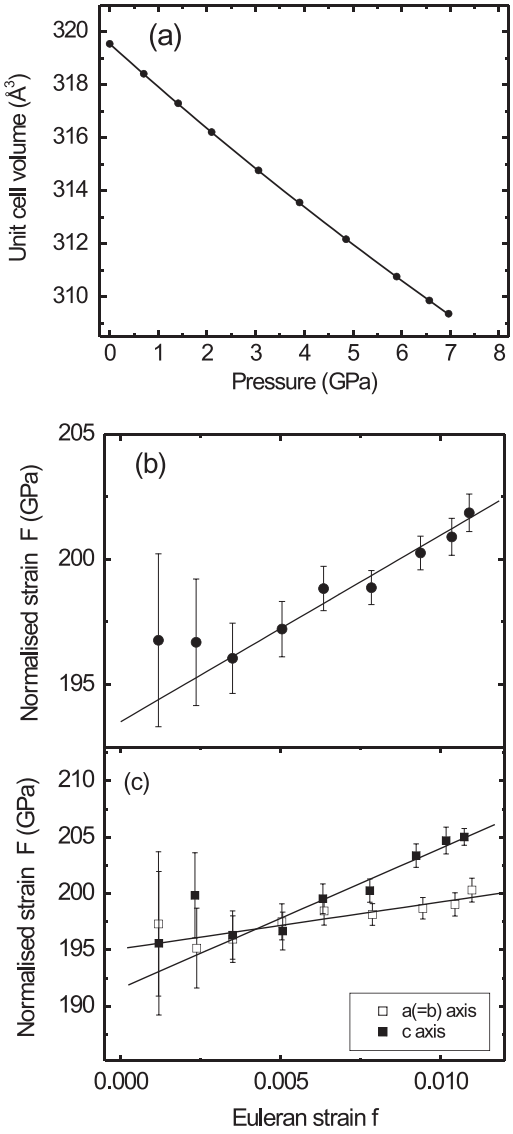

Figure 1. (a) Variation of the unit-cell volume of $PrAlO_3$ as a function pressure. The line is the third-order Birch–Murnaghan EoS fit to the data. (b) Normalized stress–strain plot derived from the measured P–V data and the Birch–Murnaghan EoS. (c) Normalized stress–strain plots from the measured cell parameters and the Birch–Murnaghan EoS. In parts (b) and (c) the slopes of the f–F plots of the data are equal to $\frac{3}{2}K_0(K' - 4)$ (Angel 2000).

parameters representing the possible distortions of the structure. The spontaneous strain components for the possible phase transitions in $PrAlO_3$ can be specified relative to the aristotype structure with $Pm\bar{3}m$ symmetry. It is more convenient for these calculations to be performed on the pseudo-cubic rhombohedral setting of the unit-cell, in which $a = b = c$ and $\alpha = \beta = \gamma$. The pseudo-cubic cell is related to the hexagonal cell by the vector equations:

$$\begin{aligned} \mathbf{a}_{pc} &= -\tfrac{2}{3}\mathbf{a}_{hex} - \tfrac{1}{3}\mathbf{b}_{hex} + \tfrac{1}{6}\mathbf{c}_{hex} \\ \mathbf{b}_{pc} &= +\tfrac{1}{3}\mathbf{a}_{hex} - \tfrac{1}{3}\mathbf{b}_{hex} + \tfrac{1}{6}\mathbf{c}_{hex} \\ \mathbf{c}_{pc} &= +\tfrac{1}{3}\mathbf{a}_{hex} + \tfrac{2}{3}\mathbf{b}_{hex} + \tfrac{1}{6}\mathbf{c}_{hex}. \end{aligned} \tag{4}$$

Table 2a. Refinement information for $PrAlO_3$ at high pressure.

P (GPa)	0.0001	0.700(3)	1.407(6)	2.094(4)	3.060(5)	3.904(6)	4.859(5)	5.896(7)	6.965(7)
$N(I > 2I_0/\sigma(I_0))$[a]	321	307	305	319	313	310	303	284	291
$N(F^2 > 2\sigma(F^2))$[b]	79	87	87	91	87	86	86	86	86
R_{int} [c]	0.030	0.033	0.043	0.037	0.043	0.046	0.047	0.044	0.042
G_{fit} [d]	1.05	1.20	1.14	1.07	0.90	0.94	1.08	1.11	0.95
Extinction factor ($\times 10^{-4}$)	0.63(7)	0.71(8)	0.57(8)	0.58(6)	0.55(6)	0.53(6)	0.62(9)	0.49(7)	0.48(5)
R_w [e]	0.036	0.040	0.040	0.038	0.032	0.035	0.040	0.040	0.035
R_u [f]	0.028	0.029	0.031	0.028	0.025	0.027	0.029	0.027	0.024

[a] Number of reflections with $I > 2I_0/\sigma(I_0)$.
[b] Number of independent reflection with $F^2 > 2\sigma(F^2)$.
[c] Internal residual for symmetry-equivalent intensities.
[d] Estimated standard deviation of unit weight observation.
[e] Weighted $R_w = [\sum w(|F_0| - |F_c|)^2 / \sum |F_0|^2]^{1/2}$, weight $w = [\sigma_i^2(F_i) + p^2F_i^2]^{-2}$.
[f] Unweighted $R_u = \sum ||F_0| - |F_c|| / \sum |F_0|$.

Table 2b. Refined positional parameters and anisotropic temperature factors and equivalent isotopic temperature factors (B_{eq}) of $PrAlO_3$ perovskite at high pressure.

P (GPa)	0.0001	0.700(3)[a]	1.407(6)	2.094(4)[a]	3.060(5)	3.904(6)[a]	4.859(5)	5.896(7)	6.965(7)[a]
Pr[b]									
B_{eq}	0.34(4)	0.39(4)	0.44(4)	0.35(3)	0.37(3)	0.36(3)	0.40(4)	0.37(4)	0.35(3)
β_{11}	0.0040(6)	0.0045(5)	0.0045(7)	0.0033(5)	0.0036(5)	0.0036(5)	0.0036(6)	0.0033(6)	0.0032(5)
β_{33}	0.000 50(10)	0.000 61(10)	0.000 82(12)	0.000 73(10)	0.000 75(9)	0.000 70(9)	0.000 89(11)	0.000 84(11)	0.000 75(9)
Al[c]									
B_{eq}	0.36(9)	0.48(11)	0.56(11)	0.50(10)	0.57(9)	0.51(10)	0.51(11)	0.61(12)	0.49(10)
β_{11}	0.0061(17)	0.0057(19)	0.0061(19)	0.0050(18)	0.0060(15)	0.0070(17)	0.0033(18)	0.0050(18)	0.0044(16)
β_{33}	0.0000(5)	0.0006(6)	0.0010(6)	0.0010(6)	0.0010(5)	0.0006(6)	0.0015(6)	0.0015(7)	0.0011(6)
O[d]									
x	0.5477(14)	0.5459(15)	0.5477(16)	0.5463(14)	0.5458(12)	0.5457(12)	0.5433(15)	0.5446(15)	0.5429(12)
B_{eq}	0.43(12)	0.43	0.60(12)	0.43	0.49(13)	0.43	0.41(15)	0.39(14)	0.43
β_{11}	0.0038(15)	0.0038	0.0072(18)	0.0038	0.0031(15)	0.0038	0.0026(18)	0.0021(19)	0.0038
β_{22}	0.002(3)	0.002	0.002(3)	0.002	0.011(4)	0.002	0.005(4)	0.006(4)	0.002
β_{33}	0.0011(4)	0.0011	0.0013(5)	0.0011	0.0007(4)	0.0011	0.0010(5)	0.0009(5)	0.0011
β_{23}	0.0004(6)	0.0004	−0.0016(8)	0.0004	−0.0008(7)	0.0004	−0.0015(9)	−0.0007(9)	0.0004

[a] Anisotropic temperature factors β_{ij} of oxygen at room pressure were used and fixed in refinements.
[b] Pr: $x = 0.0$, $y = 0.0$, $z = 0.25$, $\beta_{22} = \beta_{11}$, $\beta_{12} = 0.5\beta_{11}$, $\beta_{13} = \beta_{23} = 0$.
[c] Al: $x = 0.0$, $y = 0.0$, $z = 0.0$, $\beta_{22} = \beta_{11}$, $\beta_{12} = 0.5\beta_{11}$, $\beta_{13} = \beta_{23} = 0$.
[d] O: x, $y = 0.0$, $z = 0.25$, $\beta_{12} = 0.5\beta_{22}$, $\beta_{13} = 0.5\beta_{23}$.

Table 2c. Interatomic distance and tilting angles of $PrAlO_3$ at high pressure.

P (GPa)	0.0001	0.700(3)	1.407(6)	2.094(4)	3.060(5)	3.904(6)	4.859(5)	5.896(7)	6.965(7)
Al–O (Å^3) $x6$	1.8983(10)	1.8949(10)	1.8939(11)	1.8907(10)	1.8875(8)	1.8850(10)	1.8807(10)	1.8787(10)	1.8748(7)
Pr–O_1 (Å) $x3$	2.412(7)	2.419(8)	2.406(9)	2.411(7)	2.410(6)	2.407(6)	2.417(8)	2.406(7)	2.411(6)
Pr–O_{21} (Å) $x3$	2.921(7)	2.908(8)	2.914(9)	2.903(7)	2.896(6)	2.892(6)	2.875(8)	2.878(7)	2.864(6)
Pr–O_{22} (Å) $x6$	2.6663(7)	2.6624(7)	2.6602(8)	2.6564(7)	2.6521(6)	2.6487(8)	2.6437(7)	2.6404(7)	2.6357(5)
O–Al–O (deg)	90.78(3)	90.74(3)	90.77(3)	90.75(3)	90.74(2)	90.73(3)	90.68(3)	90.70(3)	90.67(2)
ω (deg)	9.69(31)	9.34(31)	9.69(31)	9.38(27)	9.25(23)	9.23(23)	8.81(28)	9.06(27)	8.67(21)
V_{Al_oct} (Å^3)	9.071(18)	9.069(16)	9.055(17)	9.010(14)	8.964(12)	8.928(12)	8.867(14)	8.839(14)	8.784(10)
V_{Pr_poly} (Å^3)	43.91(10)	44.00(9)	43.83(10)	43.69(8)	43.50(7)	43.33(7)	43.16(8)	42.95(8)	42.78(6)
η	0.9798	0.9807	0.9798	0.9805	0.9808	0.9809	0.9822	0.9816	0.9825

In this setting, the spontaneous strain components are then (Carpenter *et al* 2005):

$$e_1 = e_2 = e_3 = a_{pc}/a_0 - 1 \tag{5}$$

$$e_4 = e_5 = e_6 = \frac{a_{pc}\cos\alpha_{pc}}{a_0}. \tag{6}$$

The spontaneous strain components $e_1 = e_2 = e_3$ are purely non-symmetry breaking for the $Pm\bar{3}m$ to $R\bar{3}c$ transition, but they cannot be evaluated at high pressure because we have no basis with which to estimate a_0. The components $e_4 = e_5 = e_6$ are symmetry breaking. In the absence of a value for a_0, we make the approximations $e_4 = e_5 = e_6 \approx \cos\alpha_{pc}$, which are then purely symmetry breaking. The value of e_4 for $PrAlO_3$ is further from zero than that for $LaAlO_3$, confirming that the $R\bar{3}c$ phase of $PrAlO_3$ deviates further from cubic symmetry. The slope of e_4 with pressure is $+2.5 \pm 0.5 \times 10^{-5}$ GPa^{-1} (figure 3) which confirms

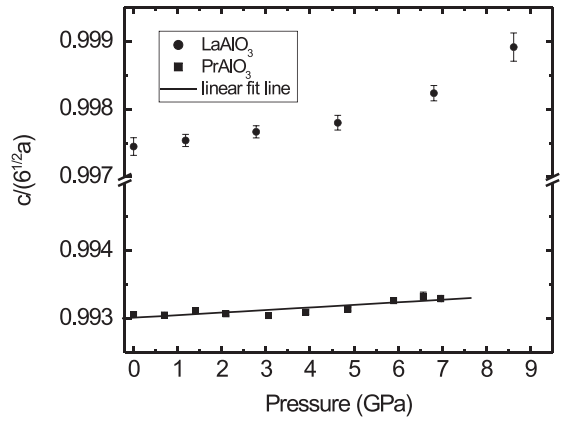

Figure 2. Variation of the ratio of unit-cell parameters $c/a\sqrt{6}$ of $LaAlO_3$ (top) and $PrAlO_3$ (bottom) with pressure.

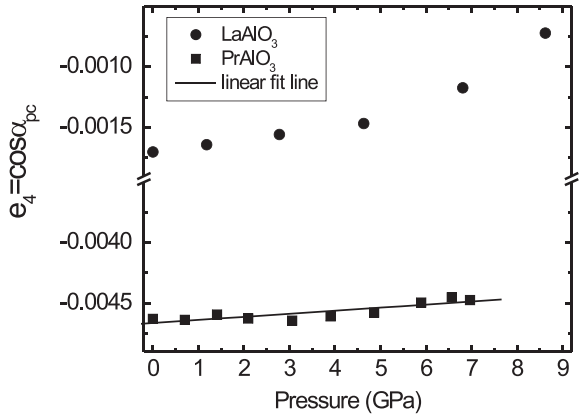

Figure 3. Variation of the spontaneous strain e_4 of $LaAlO_3$ (top) and $PrAlO_3$ (bottom) with pressure. The line is a straight-line fit to the data, and has a slope of $2.5(5) \times 10^{-5}$ GPa^{-1}.

that the unit-cell of $PrAlO_3$ evolves towards a cubic metric with increasing pressure. Figure 3 shows that this evolution is slower in $PrAlO_3$ than in $LaAlO_3$.

3.2. Structural evolution of PrAlO3

As expressed in equation (3), the key factor that determines the structural evolution of $PrAlO_3$ is the relative compressibility of the Al–O and Pr–O bonds. The variations of the Al–O bond length and average Pr–O bond length with increasing pressure are shown in figure 4. The mean linear compressibilities β_{ij} (i = Al, Pr and j = O) of both polyhedra are calculated using relation $-1/R_{ij}(0)\,\mathrm{d}R_{ij}/\mathrm{d}P$, where $R_{ij}(0)$ is the average bond length at room pressure and $\mathrm{d}R_{ij}/\mathrm{d}P$ is the slope of the average bond length. The Al–O bond ($\beta_{\mathrm{AlO}} = 1.81(8) \times 10^{-3}$ GPa^{-1}) is more compressible than the average Pr–O bond ($\beta_{\mathrm{PrO}} = 1.61(22) \times 10^{-3}$ GPa^{-1}). This is consistent with the bulk modulus of octahedral AlO_6 being smaller than polyhedral PrO_{12} (see table 1b). As a consequence, the tilt angle ω of the AlO_6 octahedra decreases with pressure (figure 5(a)), as it does for $LaAlO_3$ perovskite (Zhao *et al* 2004b). Linear extrapolation of the square of the tilt angle to zero suggests that the transition from $R\bar{3}c$ to $Pm3m$ might occur at 39 ± 3 GPa. The previous report of the octahedra being stiffer than the PrO_{12} polyhedra

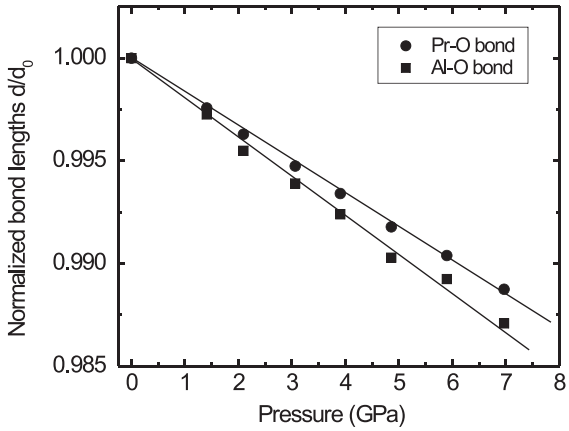

Figure 4. Variation of normalized average Al–O and Pr–O bond lengths of $PrAlO_3$ as a function of pressure.

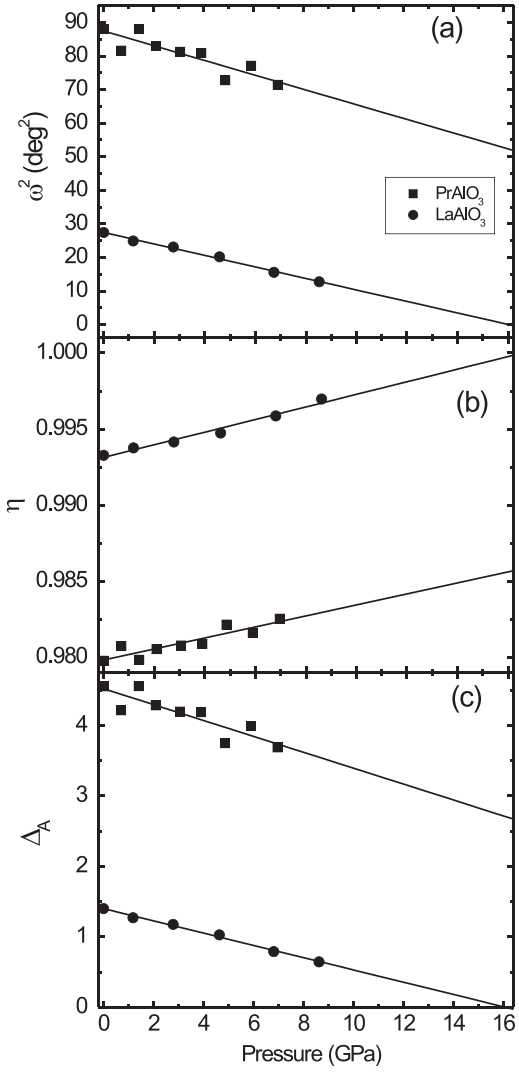

Figure 5. (a) The tilt angle ω^2, (b) and (c) distortion parameters η and Δ_A of $PrAlO_3$ and $LaAlO_3$ as a function of pressure. Lines are the linear least-square fits to the data.

in $PrAlO_3$ (figure 4(a) in (Kennedy *et al* 2002)), even though the tilt angle ω decreases, appears to be the result of an error in calculation.

Other structural parameters of $PrAlO_3$ also evolve towards cubic symmetry with increasing pressure. The strain parameter $\eta = c\cos\omega/a\sqrt{6}$ (e.g. Megaw and Darlington 1975, Thomas 1996) was introduced to describe the octahedral distortion. A value of $\eta > 1$ indicates that the octahedra are elongated along the threefold rotation axis, whereas if $\eta < 1$, they are compressed. A value of $\eta = 1$ corresponds to the completely regular octahedra found in the cubic aristotype structure. The strain parameter η of $PrAlO_3$ increases with pressure towards more regular octahedra (figure 5(b)) similar to $LaAlO_3$ perovskite. The distortion of the PrO_{12} polyhedron can be quantified by:

$$\Delta_i = (10^3/n)\sum\{(R_{ij} - \langle R_i\rangle)/\langle R_i\rangle\}^{1/2} \qquad (7)$$

in which $\langle R_i\rangle$ is the average bond length, R_{ij} is an individual bond length and n is the number of bonds (Sasaki *et al* 1983). The value for $PrAlO_3$ decreases towards the value of zero expected for the regular coordination that would be found in the cubic structure (figure 5(c)).

At ambient pressure the $R\bar{3}c$ phase of $PrAlO_3$ is stable between 215 K, below which it transforms to a structure with $Imma$ symmetry, and 1864(30) K above which it is expected to become cubic, $Pm\bar{3}m$ (Carpenter *et al* 2005, Howard *et al* 2000). Over this entire temperature range the structure evolves towards cubic symmetry with decreasing octahedral tilts, and decreasing structural distortions with increasing temperature (figure 6, (Carpenter *et al* 2005, Howard *et al* 2000)). The evolution of the $R\bar{3}c$ structure of $PrAlO_3$ with increasing pressure is thus the same as that with increasing temperature (Angel 2000), with a 40 K temperature change resulting in approximately the same change in the square of the tilt angle as a 1 GPa change in pressure. This is very similar to $LaAlO_3$, for which dT/dP is 35 K GPa^{-1}.

3.3. High-pressure phase transition

It has been reported, on the basis of powder diffraction, that $PrAlO_3$ undergoes a phase transition from $R\bar{3}c$ to $Imma$ at a pressure between 7.14 and 8.05 GPa (Kennedy *et al* 2002). In our experiments, the compression of single crystals above 7.5 GPa leads to irreversible broadening of the x-ray diffraction maxima. The geometry of the experiment allows us to exclude bridging of the anvils by the sample as the cause of this broadening, and the pressure medium remains hydrostatic to 10 GPa (Angel *et al* 2006). The reflections would not be broadened by a transition to cubic $Pm\bar{3}m$ symmetry, and there is no mechanism other than a phase transition that would generate domains within the homogeneous crystal. We therefore attribute the reflection broadening to a reduction of symmetry and the formation of multiple twin domains within the former single crystal as a result of the transition reported by Kennedy *et al* (2002). It is not possible to independently establish the symmetry of the high-pressure phase from our experimental data, but several observations are consistent with the interpretation of the powder data (Kennedy *et al* 2002) that it has the same $Imma$ symmetry as the low-temperature phase. A careful survey of reciprocal space with an area detector showed that there are no additional reflections. This eliminates

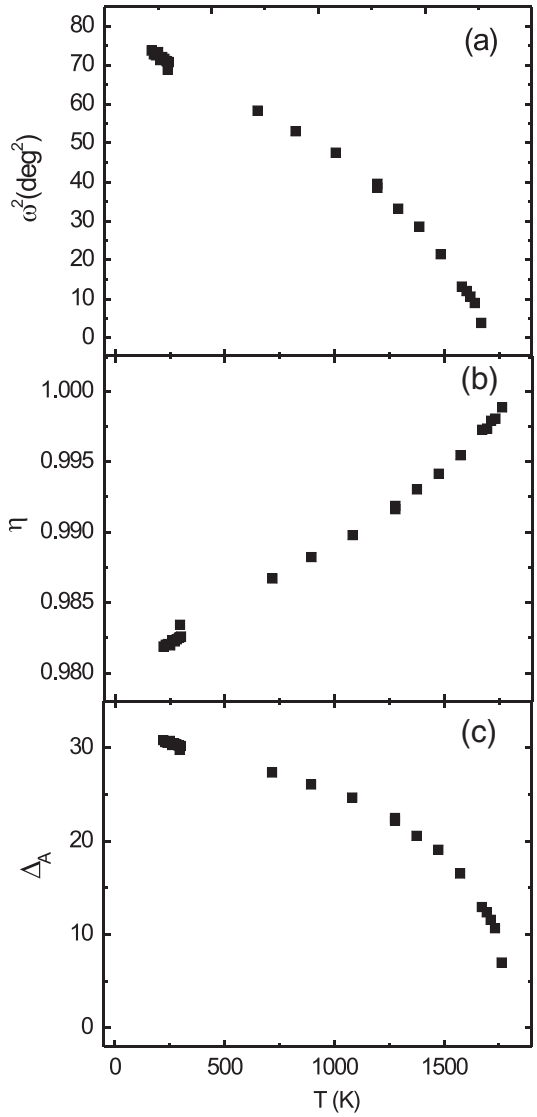

Figure 6. (a) The rotation angle ω^2, (b) and (c) distortion parameters η and Δ_A of $PrAlO_3$ as a function of temperature. Calculated from data in Howard *et al* (2000).

the possible space groups (Carpenter *et al* 2005) $P4/mmm$, $Pmmm$, and $C2/m$, but is consistent with a change in lattice from R to I-orthorhombic, as this results in the same topology of lattice points. Refinements to the intensity data collected above the phase transition can be successfully completed in $R\bar{3}c$ symmetry, indicating that the structural distortions from an average structure with $R\bar{3}c$ symmetry are small, at least within 0.2 GPa of the transition. This also explains why we did not observe the violations of the c-glide diffraction condition that would be expected after a transformation to $Imma$ symmetry. When the diffraction pattern of the high-pressure phase is indexed on the rhombohedral cell it shows, relative to the true $R\bar{3}c$ unit-cell just below the transition, a small contraction in the a cell parameter and an expansion in the c cell parameter. Thus the pattern of spontaneous strain is the same as that observed at the $R\bar{3}c$ to $Imma$ transition at low temperature (Carpenter *et al* 2005). The reflection broadening, unfortunately, prevents the measurement of unit-

cell parameters to sufficient precision that would allow the determination of the thermodynamic character of the reported transition (Kennedy *et al* 2002).

On the basis of factor group analysis, five Raman-active modes of $R\bar{3}c$ group of perovskite, $A_{1g} + 4E_g$, have been assigned (Harley *et al* 1973, Scott 1969). This is consistent with experimental Raman spectra of rhombohedral $LaAlO_3$ (Bouvier and Kreisel 2002, Scott 1969), $NdAlO_3$ (Scott 1969), and $PrAlO_3$ (Harley *et al* 1973). Figure 7(a) shows the Raman spectra of $PrAlO_3$ from 1.76 to 8.43 GPa. Three Raman modes of the $R\bar{3}c$ phase of $PrAlO_3$ (labeled in figure 7(a)) were identified. The E_g mode below 100 cm^{-1} could not be recognized due to the high background from Rayleigh scattering. Figure 7(b) shows the change of the Raman shift of these three bands as a function of pressure. The Raman mode A_{1g} that is related to the tilt of the AlO_6 octahedra (Harley *et al* 1973), and is initially at 213 cm^{-1}, softens continuously as pressure is increased from room pressure up to 7 GPa, which is similar to the A_{1g} mode of $LaAlO_3$ with both increasing pressure (Bouvier and Kreisel 2002) and temperature (Scott 1969). This is consistent with a decrease in the octahedral tilt angle with pressure (figure 5(a)). However, unlike $LaAlO_3$ whose A_{1g} mode softens towards zero as the $R\bar{3}c$ phase continuously evolves towards $Pm\bar{3}m$ symmetry (Bouvier and Kreisel 2002), the A_{1g} mode of $PrAlO_3$ hardens above 7.5 GPa following the phase transition (figure 7(b)), indicating that the decrease in the octahedral tilt towards the cubic phase has been interrupted. The E_g Raman mode around 160 cm^{-1}, related to in-plane Pr and O shifts in the $R\bar{3}c$ phase (Harley *et al* 1973) hardens below 7 GPa (figure 7(b)) and then begins to soften above 7 GPa. This is similar to the temperature-induced variation of the same Raman mode at room pressure that hardens as temperature is decreased, but softens below the phase transition to the *Imma* phase (Harley *et al* 1973). The changes in the Raman spectra at high pressures therefore mimic quite closely those associated with the low-temperature phase transition in $PrAlO_3$ perovskite (Birgeneau *et al* 1974, Lyons *et al* 1975, Watanabe *et al* 2006).

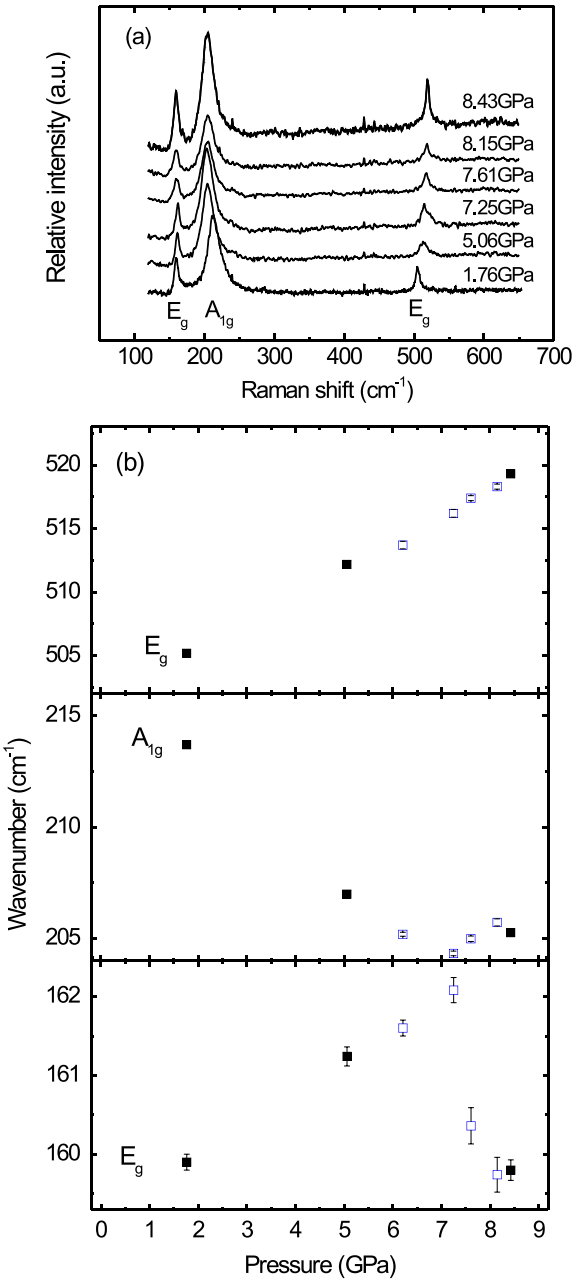

Figure 7. (a) Raman spectra of $PrAlO_3$ at different pressures; (b) changes of the Raman band positions with increasing pressure. Open symbols represent data measured during decompression from the maximum pressure.

4. Conclusions

This structural study confirms that with increasing pressure the unit-cell and structure of $PrAlO_3$ both initially evolve towards the ideal perovskite structure with $Pm\bar{3}m$ symmetry, as do other perovskites with +3 cations (Angel *et al* 2007, Ross *et al* 2004a, 2004b). However, $PrAlO_3$ is more distorted than $LaAlO_3$ at room condition and it evolves more slowly towards the cubic phase than $LaAlO_3$. This is because the site compressibility parameter M_A/M_B for $PrAlO_3$ is 1.18 at room conditions, meaning that the PrO_{12} and AlO_6 polyhedra have very similar compressibilities as observed. By contrast $M_A/M_B = 1.34$ for $LaAlO_3$ (Zhao *et al* 2004b), and the structure evolves more rapidly towards cubic symmetry because the AlO_6 octahedra are significantly softer in this material.

The two $R\bar{3}c$ perovskites $PrAlO_3$ and $LaAlO_3$ also behave essentially identically from the thermodynamic point of view. Our estimate of 39 ± 3 GPa for the pressure of the $R\bar{3}c$ to $Pm\bar{3}m$ phase transition at room temperature in $PrAlO_3$, together with the transition temperature of 1864±30 K at room pressure (Carpenter *et al* 2005, Howard *et al* 2000), yields a slope for the $R\bar{3}c = Pm\bar{3}m$ phase boundary $dT_c/dP_c = -40 \pm 4$ K GPa^{-1}. The slope for $LaAlO_3$ is -35 ± 3 K GPa^{-1}. At temperatures in excess of the saturation temperature, the slope of the phase boundary is directly related to the strength of the coupling coefficient, λ, between the tilts of the octahedra and the volume strain (equation 46 in Carpenter 2007) as $2\lambda/aK_c = dT_c/dP_c$ in which K_c is the bulk modulus of the cubic phase, and a the first coefficient in the Landau expansion

of the free energy with temperature (Carpenter 2007). Thus, the similarity in the slopes of the phase boundaries indicates that the microscopic mechanisms that drive the evolution of the structures of $PrAlO_3$ and $LaAlO_3$ with pressure, and the transitions, are essentially the same.

The single-crystal diffraction data and Raman data reported in this paper are consistent with the interpretation by Kennedy *et al* (2002) of high-pressure powder data that $PrAlO_3$ undergoes a transformation from $R\bar{3}c$ to $Imma$ at pressures in excess of 7 GPa. Given that, prior to the transition, the structure of $PrAlO_3$ evolves in the same way with *increasing* pressure as with *increasing* temperature, it is clear that the transition is not triggered by a critical value of the tilt of the octahedra, as they are becoming less tilted at high pressures, but more tilted at low temperatures. Instead, the driving force for the transition at high pressure must then simply be the reduction in volume associated with the transition to the $Imma$ phase, that is also observed at low temperatures. The negative volume strain arises from the coupling between the electronic distortion and the tilting in the $Imma$ phase (Carpenter and Howard 2009b, 2009a). The presence of an electronic component in this transition explains why it does not follow the general rules for pure tilt transitions in perovskites (Angel *et al* 2005).

Acknowledgments

The high-pressure diffraction study was performed at Virginia Polytechnic Institute and State University with the support of NSF grant EAR-0738692 to N L Ross and R J Angel. The support of the Leverhulme foundation in the form of a Visiting Professorship for CJH is gratefully acknowledged. D A Pawlak and T Lukasiewicz thank the Ministry of Science and Higher Education of Poland for support (grant No. N 5076 143 32/4056). Ruby pressure measurements and Raman spectra were conducted with the Raman system in the Vibrational Spectroscopy Laboratory in the Department of Geosciences at Virginia Polytechnic Institute and State University.

References

Ahart M, Somayazulu M, Cohen R E, Ganesh P, Dera P, Mao H K, Hemley R J, Ren Y, Liermann P and Wu Z 2008 Origin of morphotropic phase boundaries in ferroelectrics *Nature* **451** 545

Angel R J 2000 Equations of state *Reviews in Mineralogy and Geochemistry* vol 41, ed R M Hazen and R T Downs (Washington, DC: Mineralogical Society of America) p 35

Angel R J 2003 Automated profile analysis for single-crystal diffraction data *J. Appl. Crystallogr.* **36** 295

Angel R J 2004 Absorption corrections for diamond-anvil pressure cells implemented in the software package Absorb 6.0 *J. Appl. Crystallogr.* **37** 486

Angel R J, Allan D R, Miletich R and Finger L W 1997 The use of quartz as an internal pressure standard in high-pressure crystallography *J. Appl. Crystallogr.* **30** 461

Angel R J, Bujak M, Zhao J, Gatta G D and Jacobsen S D 2006 Effective hydrostatic limits of pressure media for high-pressure crystallographic studies *J. Appl. Crystallogr.* **40** 26

Angel R J, Zhao J and Ross N L 2005 General rules for predicting phase transitions in perovskites due to octahedral tilting *Phys. Rev. Lett.* **95** 025503

Angel R J, Zhao J, Ross N L, Jakeways C V, Redfern S A T and Berkowski M 2007 High-pressure structural evolution of a perovskite solid solution $(La_{1-x}Nd_x)GaO_3$ *J. Solid State Chem.* **180** 3408

Birgeneau R J, Kjems J K, Shirane G and Van Uitert L G 1974 Cooperative Jahn–Teller phase transition in $PrAlO_3$ *Phys. Rev.* B **10** 2512

Bouvier P and Kreisel J 2002 Pressure-induced phase transition in $LaAlO_3$ *J. Phys.: Condens. Matter* **14** 3405

Carpenter M A 2007 Elastic anomalies accompanying phase transitions in (Ca, Sr)TiO_3 perovskites: part I. Landau theory and a calibration for $SrTiO_3$ *Am. Mineral.* **92** 309

Carpenter M A and Howard C J 2009a Symmetry rules and strain/order-parameter relationships for coupling between octahedral tilting and cooperative Jahn–Teller transitions in ABX_3 perovskites. I. Theory *Acta Crystallogr.* B **65** 134

Carpenter M A and Howard C J 2009b Symmetry rules and strain/order-parameter relationships for coupling between octahedral tilting and cooperative Jahn–Teller transitions in ABX_3 perovskites. II. Application *Acta Crystallogr.* B **65** 147

Carpenter M A, Howard C J, Kennedy B J and Knight K S 2005 Strain mechanism for order-parameter coupling through successive phase transitions in $PrAlO_3$ *Phys. Rev.* B **72** 024118

Finger L W and King H 1978 A revised method of operation of the single-crystal diamond cell and the refinement of the structure of NaCl at 32 kbar *Am. Mineral.* **63** 337

Finger L W and Prince E 1975 A system of Fortran IV computer program for crystal structure computations *NBS, Technical Note, 854* United State National Bureau of Standards, Washington, DC

Frantti J, Fujioka Y and Nieminen R M 2007 Pressure-induced phase transitions in $PbTiO_3$: a query for the polarizatio rotation theory *J. Phys. Chem.* B **111** 4287

Hammonds K D, Bosenick A, Dove M T and Heine V 1998 Rigid unit modes in crystal structures with octahedrally coordinated atoms *Am. Mineral.* **83** 476

Harley R T, Hayes W, Perry A M and Smith S R P 1973 The phase transitions of $PrAlO_3$ *J. Phys. C: Solid State Phys.* **6** 2382

Howard C J, Kennedy B J and Chakoumakos B C 2000 Neutron powder diffraction study of rhombohedral rare-earth aluminates and the rhombohedral to cubic phase transition *J. Phys.: Condens. Matter* **12** 349

Howard C J and Stokes H T 2005 Structures and phase transitions in perovskites—a group-theoretical approach *Acta Crystallogr.* A **61** 93

Janolin P-E, Bouvier P, Kreisel J, Thomas P A, Kornev I A, Bellaiche L, Crichton W, Hanfland M and Dkhil B 2008 High-pressure effect $PbTiO_3$: an investigation by Raman and x-ray scattering up to 63 GPa *Phys. Rev. Lett.* **101** 237601

Kennedy B J, Vogt T, Martin C D, Parise J B and Hriljac J A 2002 Pressure-induced phase transition in $PrAlO_3$ *Chem. Mater.* **14** 2644

Lyons K B, Birgeneau R J, Blount E I and Van Uitert L G 1975 Electronic excitations in $PrAlO_3$ *Phys. Rev.* B **11** 891

Mao H K, Xu J and Bell P M 1986 Pressure gauge to 800 kbar under quasi-hydrostatic conditions *J. Geophys. Res.* **91** 4673

Megaw H D and Darlington C N W 1975 Geometrical and structural relations in the rhombohedral perovskites *Acta Crystallogr.* A **31** 161

Mihailova B, Angel R J, Welsch A-M, Zhao J, Engel J, Paulmann C, Gospodinov M, Ahsbahs H, Stosch R, Guettler B and Bismayer U 2008 Pressure-induced phase transition in $PbSc_{0.5}Ta_{0.5}O_3$ as a model Pb-based perovksite-type relaxor ferroelectric *Phys. Rev. Lett.* **101** 017602

Miletich R, Allan D R and Kuhs W 2000 High-pressure single-crystal techniques *Reviews in Mineralogy and Geochemistry* vol 41, ed R M Hazen and R T Downs (Washington, DC: Mineralogical Society of America) p 445

Pawlak D A, Lukasiewicz T, Carpenter M, Malinowski M, Diduszko R and Kisielewski J 2005 Czochralski crystal growth and spectroscopic properties of $PrAlO_3$ perovskite *J. Cryst. Growth* **282** 260

Ross N L, Zhao J and Angel R J 2004a High-pressure single-crystal x-ray diffraction study of $YAlO_3$ perovskite *J. Solid State Chem.* **177** 1276

Ross N L, Zhao J, Burt J B and Chaplin T D 2004b Equations of state of $GdFeO_3$ and $GdAlO_3$ perovskites *J. Phys.: Condens. Matter* **16** 5721

Sasaki S, Prewitt C T and Liebermann R C 1983 The crystal structure of $CaGeO_3$ perovskite and the crystal chemistry of the $GdFeO_3$-type perovskites *Am. Mineral.* **68** 1189

Scott J F 1969 Raman study of trigonal-cubic phase transitions in rare-earth aluminates *Phys. Rev.* **183** 823

Thomas N W 1996 A re-examination of the relationship between lattice strain, octahedral tilt angle and octahedral strain in rhombohedral perovskites *Acta Crystallogr.* B **52** 954

Tohei T, Kuwabara A, Yamamoto T, Oba F and Tanaka I 2005 General rule for displacive phase transitions in perovskite compounds revisited by first principles calculations *Phys. Rev. Lett.* **94** 035502

Watanabe S, Hidaka M, Yoshizawa H and Wanklyn B M 2006 Antiferroelastic structural transitions in $PrAlO_3$ by means of neutron diffraction *Phys. Status Solidi* b **243** 424

Zhao J, Ross N L and Angel R J 2004a New view of the high-pressure behaviour of $GdFeO_3$-type perovskites *Acta Crystallogr.* B **60** 263

Zhao J, Ross N L and Angel R J 2004b Polyhedral control of the rhombohedral to cubic phase transition in $LaAlO_3$ perovskite *J. Phys.: Condens. Matter* **16** 8763